NANO LETTERS

Letter

Cite This: Nano Lett. XXXX, XXX, XXX-XXX

pubs.acs.org/NanoLett

Rotation and Negative Torque in Electrodynamically Bound Nanoparticle Dimers

Nishant Sule,[†] Yuval Yifat,[†] Stephen K. Gray,[‡] and Norbert F. Scherer*[,†,§]

[†]James Franck Institute, The University of Chicago, 929 E. 57th Street, Chicago, Illinois 60637, United States

[‡]Center for Nanoscale Materials, Argonne National Laboratory, 9700 South Cass Avenue, Argonne, Illinois 60439, United States

[§]Department of Chemistry, The University of Chicago, 929 East 57th Street, Chicago, Illinois 60637, United States

Supporting Information

ABSTRACT: We examine the formation and concomitant rotation of electrodynamically bound dimers (EBD) of 150 nm diameter Ag nanoparticles trapped in circularly polarized focused Gaussian beams. The rotation frequency of an EBD increases linearly with the incident beam power, reaching mean values of ∼4 kHz for relatively low incident powers of 14 mW. Using a coupled-dipole/effective polarizability model, we reveal that retardation of the scattered fields and electrodynamic interactions can lead to a "negative torque" causing rotation of the EBD in the direction opposite to that of the circular polarization. This intriguing opposite-handed rotation due to negative torque is clearly demonstrated using electrodynamics-Langevin dynamics simulations by changing particle separations and thus varying the retardation effects. Finally, negative torque is also demonstrated in experiments from statistical analysis of the EBD trajectories. These results demonstrate novel rotational dynamics of nanoparticles in optical matter using circular polarization and open a new avenue to control orientational dynamics through coupling to interparticle separation.

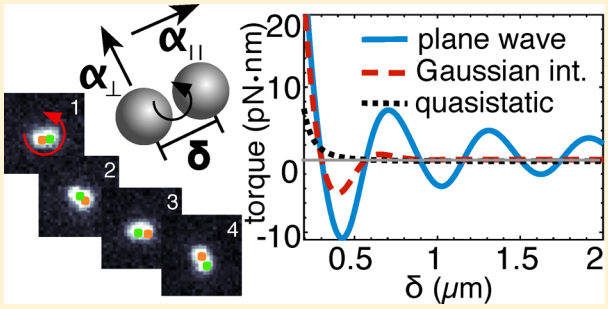

KEYWORDS: *Optical tweezers, optical trapping, plasmonic nanoparticles, optical torque, negative optical torque, angular momentum*

The development of optical trapping of micron-scale objects by Ashkin et al.[1] has heralded new fields of research ranging from optical physics[2] to molecular biology[3] and microbiology,[4] materials science,[5] and lithography.[6] Optical tweezers also allow precision measurements of the dynamics of and interactions between micro- and nanoscale particles in order to address frontier questions in statistical mechanics.[7−10] These and other studies illustrate that the trapping beam strongly affects particle behavior. Thus, there is profound interest in controlling particle dynamics with the wavelength, optical power, wavefront, cross-sectional profile, and polarization of the trapping beam.[11] In particular, the polarization state of the trapping laser provides a relatively simple means to control trapped particle behavior. As an example of this, several papers have demonstrated the use of circularly polarized light to trap and cause nanoscale objects to spin.[12−16] However, research to date has focused on the dynamics of a single particle in the trap. Except for theoretical work on nonconservative torque from a circularly polarized plane wave[17] and a recent paper concerning multiple particle assemblies,[18] the behavior of two electrodynamically interacting particles in a focused trap has not been explored.

In this Letter, we demonstrate through experiments and numerical simulations the orientational (e.g., rotational) dynamics of two 150 nm diameter particles placed in a circularly polarized and focused Gaussian trap and show that the rotational motion about their center of mass is a consequence of their self-organization into an electrodynamically bound dimer (EBD). We show that for near-field separations, where retardation is negligible, the EBD rotates like a rigid body with a direction dependent on the angular momentum of the incident circularly polarized light and that its angular velocity increases linearly with the incident optical power. We observe an average angular frequency as high as ∼4 kHz for reasonably low optical power (14 mW and a power density of 5 MW/cm^2). Furthermore, we develop an analytical model for the effective polarizability of the EBD to examine the torque imparted by circularly polarized light. This model predicts that the separation between the particles relative to the wavelength of the trapping beam determines both the magnitude and direction of the torque. For certain separations, the EBD experiences a "negative torque" due to retardation of the electric fields and electrodynamic interactions that would cause it to rotate with opposite handedness to the polarization. We demonstrate opposite-handed rotation, that is, negative torque, on the EBD in our full electrodynamics−Langevin dynamics simulations. Furthermore, using statistical analysis of long trajectories of the EBD we also observe negative torque in experiments. Our experimental evidence of negative torque in

Received: May 24, 2017
Revised: September 29, 2017
Published: September 29, 2017

DOI: 10.1021/acs.nanolett.7b02196
Nano Lett. XXXX, XXX, XXX−XXX

plasmonic systems demonstrates new opportunities to control the dynamics of driven optical matter.

Experimental and Simulation Details. The experiments were performed using a standard optical tweezers setup. A Ti:sapphire laser tuned to a wavelength of 790 nm and emitting linearly polarized light was collimated and directed into a Nikon TI inverted optical microscope and through a Nikon 60x Plan APO IR water immersion objective (NA = 1.27). The laser beam was focused into a sample cell containing 150 nm diameter Ag nanoparticles coated with a ligand layer of polyvinylpyrrolidone (PVP; NanoComposix) diluted in deionized water at a ratio of 1:200. The beam was positioned so that its focus was slightly below (before) the top coverslip and had a full width half-maximum (fwhm) of ∼500 nm at the coverslip. We controlled the polarization state of the incident light by positioning a quarter-wave plate beneath the objective and investigated the dynamics that ensued. The particles were illuminated using a dark-field condenser and their motion was captured using an sCMOS camera (Andor Neo). See Supporting Information for a schematic of the experimental setup and for more information about the Ag nanoparticles.

In order to ascertain the angular velocity of the EBDs from experiments, we employed particle tracking methods to precisely determine the locations of each of the trapped particles in the acquired time series of images (i.e., videos). Since the EBDs rotate with a high frequency (thousands of hertz), we viewed only a small region of interest in the imaging camera chip (50 × 50 pixel region), allowing the motion to be captured with an exposure time of 0.1 ms at 2004 frames per second. Each frame was tracked and linked using the nonlinear, least-squares Gaussian fitting algorithm for centroid determination (described in Sbalzarini and Koumoutsakos[19]), resulting in a table of (x, y) positions of the particles from which the interparticle separation, δ_n, and the orientation of the EBD in the lab frame, θ_n, in each frame n are calculated. The instantaneous angular velocity of the EBD, ω_n, was then calculated from the difference in the EBD orientation angle between two sequential frames, i.e. $\omega_n = (\theta_{n+1} - \theta_n)F$, where F is the frame rate.

However, due to the small size of the particles and of the interparticle separations the particle localization algorithm suffered from a Nyquist undersampling error which biased the tracked particle positions toward the center of the pixels. This effect, known as pixel-locking, along with an algorithm for correcting the error named the single particle interior filling function (SPIFF) method is described by Burov et al.[20] We used the SPIFF method to alleviate the problem and correct for errors in the measured interparticle distance and angle. Further details of the particle tracking errors and the method we applied to correct them are given in the Supporting Information and in Yifat et al.[21]

Simulations of two Ag nanoparticles in a focused Gaussian trap were performed using an in-house electrodynamics-Langevin dynamics (ED−LD) technique.[10,22] The ED−LD simulation self-consistently coupled the finite-difference time-domain (FDTD) method of solving Maxwell's equations with a splitting-method for integrating the Langevin equation. The circularly polarized focused Gaussian beam was introduced in the simulation using the scattered-field technique[23,24] where the incident electric field is as described in Novotny and Hecht.[25] See Supporting Information for expressions for the electric fields near the focal region. The incident magnetic field was calculated from Ampere's law at each time step before updating the scattered-fields in the main FDTD calculation. The electrodynamic forces on the Ag nanoparticles were calculated using the Maxwell stress tensor, while the electrostatic forces due to surface charges were calculated using Coulomb's law. The Drude model was used to describe the dispersive Ag nanoparticles using the auxiliary differential equation method.[24] The total force on each nanoparticle was used in the Langevin equation to update their positions. The trajectories were calculated by repeating the aforementioned steps.

In the simulations, we calculated the positions of the particles from the Langevin equation using a time step of 0.2−0.5 μs and therefore, the "instantaneous" angular velocities are the differences between the EBD orientation in the xy plane in successive simulations steps divided by the time step. Moreover, to allow quantitative comparison between experiment and simulations, the incident circularly polarized (CP) focused Gaussian beams in the simulations were generated with the same fwhm, power, and NA as the experiments.

Dynamics of Trapped Metal Nanoparticles. It is known that a single particle trapped in a CP focused Gaussian beam will spin due to the transfer of angular momentum from the beam to the particle.[12,15,26] For asymmetric particles, rotation could also arise from anisotropic scattering rather than polarization.[27] Moreover, it has been shown that two Ag nanoparticles in a linearly polarized (LP) trapping beam attain two configurations; a dimer structure with its axis preferentially oriented along the direction of polarization when the particles have small separations (i.e., in near-field separations) or with the interparticle axis perpendicular to the polarization when the particles are in the optical binding regime.[28,29] An example of the dimer structure in LP light is shown in Movie S1 in the Supporting Information. Yet the dynamics of two nanoparticles in a CP trap, as we show here, are more interesting and require a more nuanced explanation.

The positions of two 150 nm Ag nanoparticles illuminated by a CP focused Gaussian beam obtained from ED−LD simulations are shown in Figure 1a. The images are ordered in time from top to bottom and we show that the two Ag nanoparticles quickly (in ∼5 ms; top two frames in Figure 1a) form an EBD with near-field separations (∼195 nm center-to-center). In the near-field regime the EBD rotates about its center of mass as a rigid object with the same handedness as that of the incident CP light (bottom three frames in Figure 1a). A movie (Movie S2) of the trajectories obtained from the ED−LD simulations with right and left-handed CP beams is shown in the Supporting Information.

In experiments, two Ag nanoparticles trapped in a CP Gaussian beam fluctuate in their orientational positions when separated beyond the near-field regime and rotate strongly in the near-field regime (See Supporting Information Movie S3). Figure 1b shows the particle positions as seen in experiments using dark-field microscopy for right-handed (first column) and left-handed (second column) CP Gaussian beams (See Supporting Information, Movies S4 and S5). The EBD rotates clockwise (counterclockwise) for right-handed (left-handed) circular polarization. In other words, the particles rotate when they are in the near-field regime of separations, and their rotation direction is determined by the handedness of the circular polarization. Note that if the polarization orientation of a LP Gaussian beam is rotated (e.g., by rotating a a half-wave plate before the microscope) the EBD orientation rotates with it, but the torque would not persistently drive the EBD. If the direction of LP does not change, the EBD's orientation would

DOI: 10.1021/acs.nanolett.7b02196
Nano Lett. XXXX, XXX, XXX−XXX

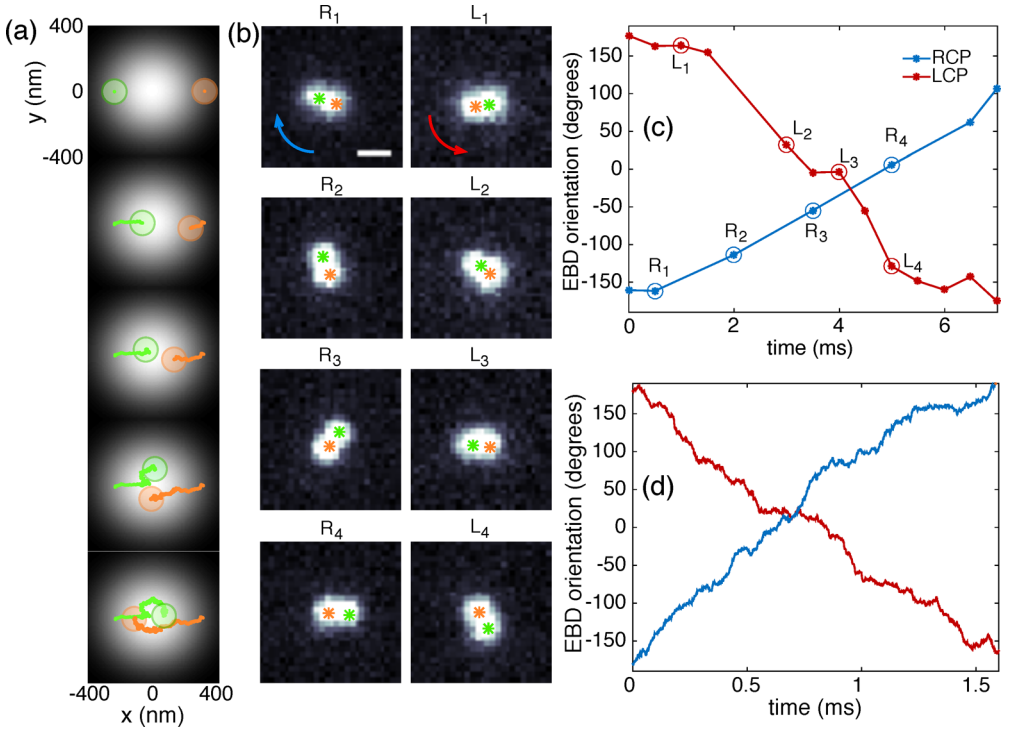

Figure 1. Formation and rotation of an EBD in a focused CP Gaussian beam. (a) Trajectories obtained from ED−LD simulation of two 150 nm diameter Ag nanoparticles illuminated by a right-handed focused CP beam depicting the formation and concomitant rotation of the EBD in the near-field (ordered from top to bottom in time). See Movie S2 depicting the ED−LD simulated trajectories in the Supporting Information. The background gradient shows the intensity distribution of the incident trapping beam (white is highest intensity). (b) Series of experimental dark-field images (ordered from top to bottom in time) of an optical dimer composed of two 150 nm diameter Ag nanoparticles rotating clockwise (left column) and counterclockwise (right column) for right-handed and left-handed CP light, respectively. Arrows designate direction of rotation of the EBD. See Movie S3 and S4 in the Supporting Information (c) Experimental and (d) simulated trajectories of the orientation of the EBD axis as a function of time for right-handed (blue) and left-handed (red) CP light (incident power is 7 mW for experimental trajectory and 12 mW for trajectories obtained from ED−LD simulation). Circled points on the graph in panel (c) (R_1, L_1 → R_4, L_4) represent selected frames shown in (b).

stay fixed. Conversely, in a CP Gaussian beam we observe persistent non-zero torque on the bound pair.

Figure 1c,d shows the change in the orientation of the EBD as a function of time from experiment (Figure 1c) and simulation (Figure 1d), for both CP handed cases. The positions from the dark-field images shown in Figure 1b are marked by labels R_1 through R_4 for right-handed and L_1 through L_4 for left-handed circularly polarized light, respectively. In contrast, when the particles are trapped with LP light, the EBD maintains an orientation along the polarization direction (with small Brownian fluctuations), as can be seen in the Supporting Information (Movie S1) in agreement with previous reports.[15,28] This is true for both our experiments and the ED−LD simulations.

A comparison of the intensity distribution of the experimental and simulated beams is shown in Figure 2a (top) along with a plot of the cross-sectional cuts of the intensity distribution through the maximum intensity (bottom).

Figure 2b shows that the angular velocity (or rate of rotation) of the EBD increases linearly with increasing optical power in both the experiments and simulations. The error bars in 2b are the standard deviation of the measured angular velocities. The standard deviations in the experimental data arise from several factors: Brownian motion of the particles, which is more significant at low power (i.e., low angular drive); jitter in the shutter timing, which determines when the camera exposure will occur and has a larger effect at higher velocities, and also errors in particle tracking. For the simulated trajectories, the standard deviations only depend on the Brownian noise, and therefore decrease with increasing optical power as the trajectories become more deterministic. Although, the fitted lines in Figure 2b clearly exhibit a linear dependence, the magnitudes of the experimentally determined angular velocities are a factor of ∼2 smaller than that obtained from simulations. We ascribe this discrepancy to the hydrodynamic interactions and friction between the particle and glass surface that are not accounted for in the simulation.

Theory for Rotational Dynamics of EBDs. To understand the rotational dynamics of the EBD, we developed an analytical model for the torque on EBDs treating each particle as a point dipole. The model reformulates the EBD as a single ellipsoidal nanoparticle with an effective polarizability calculated from the polarizabilities of the individual particles. The model accounts for the dispersive permittivity of Ag and retardation of the scattered fields. Figure 3a shows a schematic of the EBD geometry where θ is the orientation of the EBD in the x,y plane; i.e., the angle between the dimer axis (along the rotated x' coordinate axis) and the lab frame x-coordinate axis. The electric field in the lab frame is defined as $\vec{E} = E_0 e^{ikz}(\hat{x} \pm i\hat{y})$, where $k = 2\pi n/\lambda$ is the wave vector, and the $\pm$ sign denotes right-handed and left-handed CP light, respectively. Assuming identical particles and following the approach in Khlebtsov et al.[30] and Pinchuk and Schatz[31] we calculate the effective polarizability of the optical dimer along, $\alpha_{\parallel}$, and perpendicular, $\alpha_{\perp}$, to the dimer axis as

DOI: 10.1021/acs.nanolett.7b02196
Nano Lett. XXXX, XXX, XXX−XXX

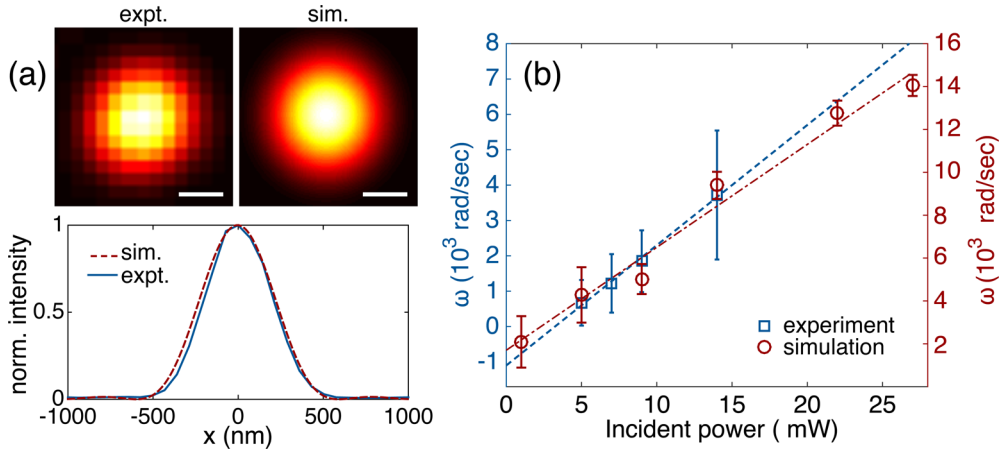

Figure 2. Dependence of the angular velocity, ω, of the EBD on the incident beam power. (a) (top panels) Intensity distribution at the focus of the trapping beam in the experiments (left) and simulations (right). The white scale bar represents 250 nm. (a) (bottom panel) The cross-section of the normalized intensity along $y = 0$ showing the nearly identical fwhm of the experimental (blue) and simulated (red dashed) beams. (b) Angular velocity of the EBD as a function of optical power of the incident beam power as measured experimentally (blue squares, left y-axis) and through numerical simulations (red circles, right y-axis). The angular velocity is calculated as the change of orientation of the optical dimer axis as a function of time interval. The time interval is the reciprocal of the frame rate for the experimental data and is 1 μs for the simulation data. The dashed (blue) and dot-dashed (red) lines are linear fits to the experimental and simulation results, respectively. They agree to better than a factor of 2. Differences may be due to variations in particle size and shape and the hydrodynamic friction with the surface present in the experiment but not in the simulations.

$$\alpha_{\parallel} = \frac{2\alpha + \frac{\alpha^2 k^3}{2\pi\epsilon_0}[A(k\delta) + B(k\delta)]}{1 - \frac{\alpha^2 k^6}{(4\pi\epsilon_0)^2}[A(k\delta) + B(k\delta)]^2} \tag{1a}$$

$$\alpha_{\perp} = \frac{2\alpha + \frac{\alpha^2 k^3}{2\pi\epsilon_0}A(k\delta)}{1 - \frac{\alpha^2 k^6}{(4\pi\epsilon_0)^2}A^2(k\delta)} \tag{1b}$$

where $\alpha = \alpha_0/[1 - \phi(k)\alpha_0]$ is the polarizability of a single sphere[25] of radius a, and δ is the center-to-center interparticle separation. The electrostatic polarizability of a sphere, α_0, is given by the Clausius-Mossotti relation, $\alpha_0 = 4\pi\epsilon_0\epsilon_m a^3(\epsilon_p - \epsilon_m)/(\epsilon_p + 2\epsilon_m)$,[25] where ϵ_p is the complex permittivity of the particle and ϵ_m that of the medium. We assume that the background medium is water with $\epsilon_m = 1.77$. The function $\phi(k) = ik^3/6\pi\epsilon_0\epsilon_m$ corrects for radiative damping. The functions $A(k\delta)$ and $B(k\delta)$

$$A(k\delta) = \left[\frac{1}{k\delta} + \frac{i}{(k\delta)^2} - \frac{1}{(k\delta)^3}\right]e^{ik\delta} \tag{2a}$$

$$B(k\delta) = \left[-\frac{1}{k\delta} - \frac{3i}{(k\delta)^2} + \frac{3}{(k\delta)^3}\right]e^{ik\delta} \tag{2b}$$

result from the dipole interaction matrix elements and take into account retardation of the scattered fields, which depends on the separation between the particles. The electric-field vector can be resolved in the sample frame of reference (i.e., the EBD frame) by multiplying with the rotation matrix, that is, $\vec{E}' = \mathrm{R}\vec{E}$ and the polarization density vector in the EBD frame can be written as $\vec{p}' = \overline{\overline{\alpha}}\vec{E}'$. The total, time averaged, torque on the EBD is then given by[32,33] $\langle\vec{\tau}\rangle = \frac{1}{2}\mathcal{R}[\vec{p}' \times (\overline{\overline{\alpha}}_0^{-1}\vec{p}')^*]$, where $\mathcal{R}$ represents the real part, * denotes the complex conjugate, and $\overline{\overline{\alpha}}_0$ is the effective polarizability matrix where the α in eq (1a,1b) is replaced by α_0. Thus, we find that the torque on the EBD from right-handed (top sign) and left-handed (bottom sign) CP is

$$\langle\vec{\tau}\rangle = \mp\frac{1}{2}|E_0|^2\mathcal{R}\left[i\left(\alpha_{\parallel}\frac{\alpha_{\perp}^*}{\alpha_{0,\perp}^*} + \alpha_{\perp}\frac{\alpha_{\parallel}^*}{\alpha_{0,\parallel}^*}\right)\right]\hat{z} \tag{3}$$

(see Supporting Information for more details).

The torque calculated from eq 3 is shown in Figure 3b–d. The curves in Figure 3b show torque on an EBD composed of two 150 nm diameter Ag nanoparticles. The solid blue curve denotes torque calculated by assuming a right-hand CP plane wave illuminating the particles. The most intriguing aspect of this curve is that for certain separations the torque becomes negative and that the positive and negative torques repeat with a periodicity of approximately the wavelength of the incident source (in our case 800 nm in vacuum or ~600 nm in water). These results are in agreement with the work by Haefner et al.[17] on nonconservative torques from CP light on two electrodynamically interacting particles about their center of mass. However, Haefner et al.[17] only examined the results for plane waves and torque at optical binding separations. When the incident source (wavelength of 800 nm) has a Gaussian intensity envelope with a fwhm of 450 nm (to approximate the conditions in experiments), we show that the torque (shown by the red dashed curve) decays more rapidly with increasing separation while still exhibiting negative torque. Although there exists a finite torque at optical binding separations, the smaller magnitude makes it difficult to observe in experiments vs the Brownian motion.

"Negative torque", which would cause the EBD to rotate with a handedness opposite to the direction of polarization of the incident beam, has recently been studied theoretically by Chen et al.[34] with micron-sized dielectric particles by considering explicit structures of 3–10 particles. The existence of negative optical torque was explained as arising from field retardation and breaking of rotational symmetry.[34] By contrast, we do not impose any specific structure and consider a simpler geometry

DOI: 10.1021/acs.nanolett.7b02196
Nano Lett. XXXX, XXX, XXX−XXX

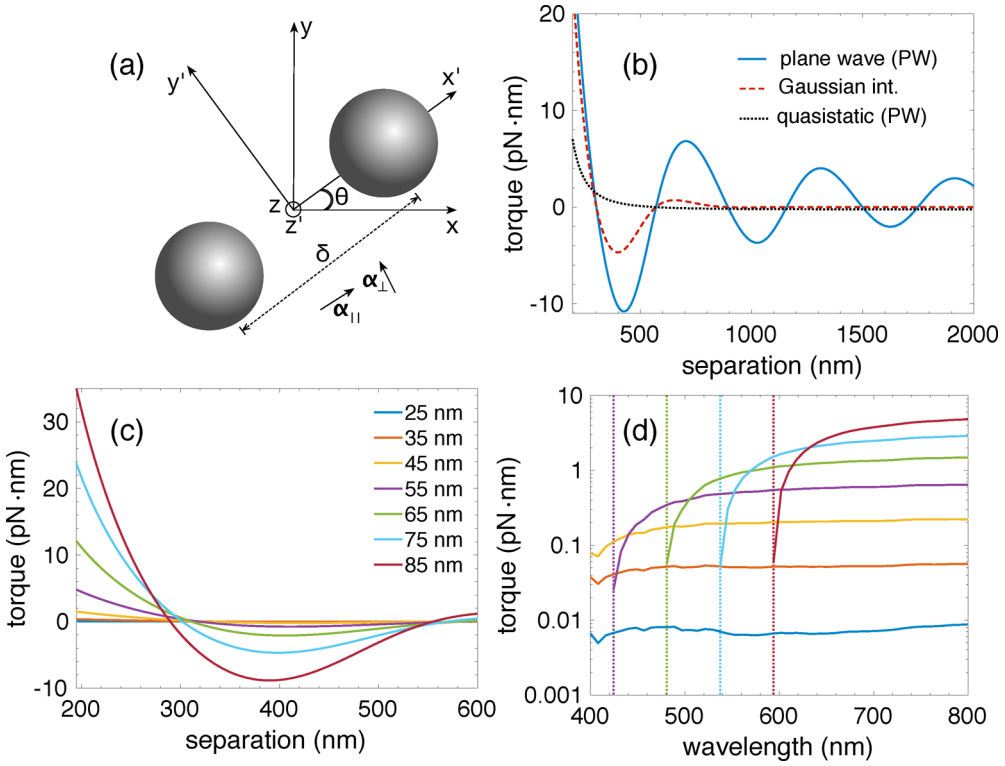

Figure 3. Analytical model for the torque on the EBD using the dipole approximation. (a) Schematic and coordinate system of an EBD. (b) Torque on the EBD as a function of the center-to-center separation of the two 150 nm diameter Ag nanoparticles. The solid blue curve shows the torque calculated by assuming that the incident source is a plane wave, the dashed red curve is for a source with a Gaussian intensity envelope, and the dotted black curve is the torque calculated under the quasistatic approximation for an incident plane wave. (c) The torque on the EBD as a function of interparticle separation, for different particle radii, from 25 to 85 nm. (d) Torque on an EBD composed of Ag nanoparticles with surface-to-surface separation of 45 nm as a function of the wavelength of the incident source with a plane wave source. The vertical dotted lines denote the wavelength at which the torque is negative. The different colors represent particles of different radii using the same color scheme as in panel (c).

with just two nanoscale particles. The Ag nanoparticle EBD does indeed break rotational symmetry with respect to the incident CP light. Moreover, if we do not take retardation effects into account (i.e., we make the quatistatic approximation that entails $k \to 0$, which makes $A(kd) \to (kd)^{-3}$, and $B(kd) \to 3(kd)^{-3}$) then the torque is always positive as seen from the black dotted curve in Figure 3b. The incident field used for calculating the black dotted curve in Figure 3b is the same as that used for the calculation of the blue curve, that is, right-hand CP plane wave. It can be seen from eqs 1a,1b and 2a,2b that retardation of the scattered fields can lead to a change in magnitude and sign of the joint-particle polarizability tensor; the magnitude and sign depend on the particle separations relative to the wavelength, giving rise to the negative torque.

Figure 3c shows the torque calculated as a function of separation, δ, between particles of different radii assuming a source with a Gaussian transverse intensity. The torque becomes negative for a center-to-center separation around 300 nm, that is, $\sim\lambda/2$, due to field retardation. The magnitude of the optical torque on the EBD increases with particle size (due to the increase in the scattering cross section) as expected. However, as the center-to-center separation, δ, between the particles increases, retardation effects result in a change in sign of the optical torque. The magnitude of negative torque for smaller particles (radii <60 nm) is negligible due to their small scattering cross sections.

Figure 3d shows the torque on the EBD in the near-field regime (i.e., surface-to-surface separation of 45 nm) as a function of wavelength of the incident field; the curves are calculated for plane wave incident fields. The different colored curves represent particles of different radii using the same color scheme as panel (c). The vertical dotted lines indicate the wavelengths at which the torque becomes negative (and therefore cannot be shown on a log scale). The gradient force pulls particles closer and the Coulomb repulsion balance at about 50 nm. For the conditions of our experiments and simulations we use a surface-to-surface separation of 45 nm for all the curves in Figure 3d, which is the near field separation regime. Thus, we predict that particles with radii of 55 nm (purple), 65 nm (green), 75 nm (light blue), and 85 nm (red) would exhibit negative torque at wavelengths of 424, 480, 537, and 594 nm, respectively, in the near-field regime.

Negative Torque in ED−LD Simulations. The analytical model described above assumes the dipole approximation to calculate the effective polarizability. However, it has been shown that the effective polarizability of a dimer calculated using the dipole approximation is not accurate even when the individual particles are considered to be small enough to be in the Rayleigh limit.[30] This is especially true for small relative separations, that is, $\delta/a < 3$.[30] Therefore, we performed full ED−LD simulations to test the prediction of the negative optical torque calculated from the analytical model. In order to observe rotation in the direction opposite to the polarization, we restricted the smallest separation that the two particles could attain by creating virtual spherical hard-sphere boundaries around the particles in the Langevin solver. These virtual boundaries only affect the minimum separation attainable and do not otherwise affect the electrodynamics or Langevin

DOI: 10.1021/acs.nanolett.7b02196
Nano Lett. XXXX, XXX, XXX−XXX

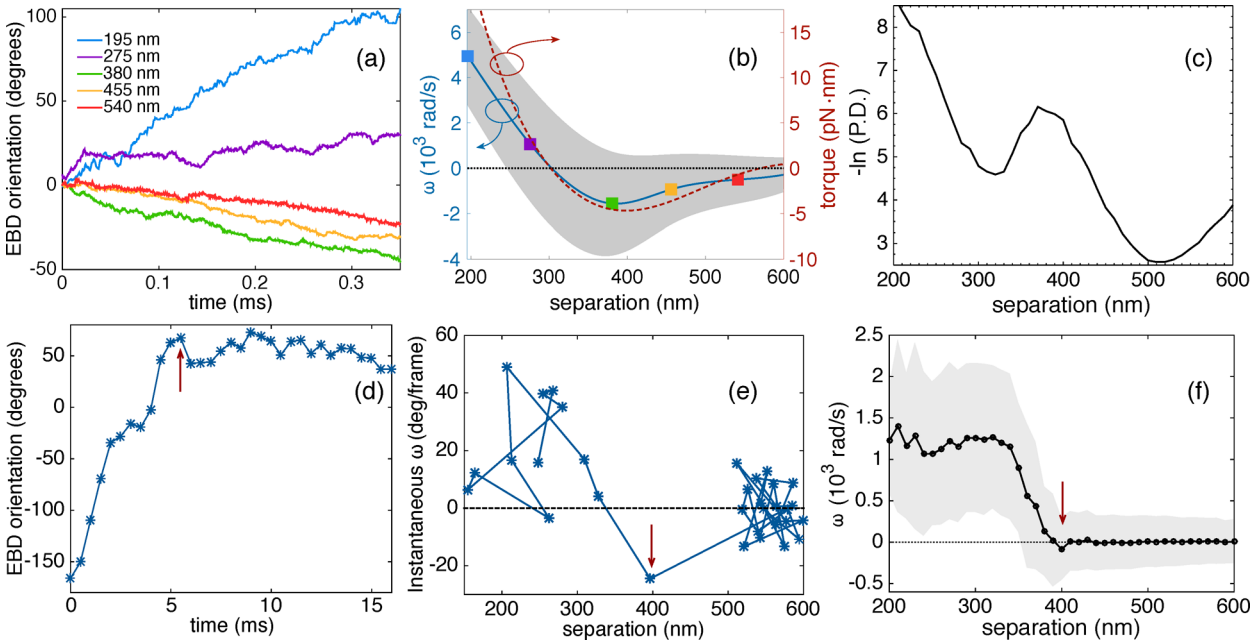

Figure 4. Negative torque on the 150 nm sized Ag nanoparticle EBD. (a) Orientation of the EBD as a function of time calculated from ED−LD simulations for different minimum separations between the particles where the incident beam is a right-hand CP focused Gaussian beam. (b) Angular velocity (squares, left *y*-axis) calculated from the trajectories obtained in the ED−LD simulations corresponding to different minimum separations between the EBD. The colored points correspond to the colors in (a). The gray shaded region represents the standard deviation from the mean values. Torque (red dashed curve, right *y*-axis) calculated from the analytical model assuming a right-hand CP incident beam with a Gaussian intensity envelope of 450 nm fwhm. (c) Potential of mean force (pmf), which is the negative natural log of the probability density, as a function of interparticle separation for the experimental data presented in panel (f). (d) An experimental trajectory showing the EBD orientation; the particles transition from the near-field region to optical binding separations at ∼5 ms. The arrow marks the transition point where the interparticle separation is 400 nm and opposite-handed rotation due to negative torque is observed. The experimental frames of this particular event are shown in the Supporting Information and in Movie S6. (e) Experimentally measured instantaneous ω for the trajectory shown in panel (d). The arrow indicates the transition point (around a separation of 400 nm) where the instantaneous ω is negative due to the negative torque. (f) Experimentally determined average angular velocity as a function of particle separation showing a signature of negative torque on the EBD at a separation of approximately 400 nm consistent with the simulation results. The gray shaded region represents the standard deviations from the mean value of ω. The arrow indicates the separation at which we observe negative torque.

dynamics of the simulation. The results of these simulations are shown in Figure 4a,b.

Figure 4a shows the orientation of the EBD in time simulated for different minimum separations between the particles. In all these simulations the incident source is a right-hand CP focused Gaussian beam and the Ag nanoparticles are 150 nm in diameter. We see that the EBD rotates in the right-handed sense for center-to-center separations of 195 and 275 nm, that is, in the direction of the CP light, whereas the EBD rotates in the left-handed or opposite sense to the CP light for separations of 455 and 540 nm. For interparticle separations of more than 350 nm, we simulated incident focused beams with higher power in order to overcome Brownian noise and obtain sufficient driven motion in the 0.35 ms long trajectory. These trajectories clearly demonstrate the intriguing effect of negative torque that causes the EBDs to rotate in the direction opposite to the handedness of the polarization.

As shown in Figure 4b, we calculated the average angular velocity (ω) from the ED−LD simulated time trajectories of the orientation of an EBD axis for different minimum separations between the particles. The angular velocity of a particle in an overdamped system increases linearly with torque (see Supporting Information for details). Therefore, to compare with our analytical model, we plot the torque on an EBD calculated using an incident field with a Gaussian intensity envelope of 450 nm fwhm given by the red dashed curve in Figure 4b. The ED−LD simulations results confirm the existence of negative optical torque as expected from the analytical model. The dipole approximation breaks down at small separations and also when higher-order modes are excited in particles larger than 150 nm. These factors lead to the small discrepancy between the analytical model and the ED−LD simulations.

Experimental Observation of Negative Torque. Observing negative optical torque in experiment is challenging due to the inherent preference of the particles to either be in the near-field regime (i.e., center-to-center separation of 200−300 nm) or the optical-binding regime (i.e., center-to-center separation of ∼600 nm). We repeated the trapping experiments described above with the addition of an iris centered before the objective. Closing the iris decreases the size of the incident beam, thereby decreasing the *NA* and alters the width and stiffness of the focused optical trap. This loosely focused Gaussian beam allows us to explore the interparticle interactions over a larger range of separations since the particles are not confined to the near-field region and may transition between the near-field and optical binding regions. An example of the particle dynamics in such a trap is shown in the Supporting Information (Movie S3) in which we observe the particles fluctuating at optical binding separation then quickly rotating as they approach each other at separations less than 400 nm. By recording long videos we can observe particles inhabiting both regimes, as well as the transitions between them. As the potential mean force (i.e., the negative logarithm

DOI: 10.1021/acs.nanolett.7b02196
Nano Lett. XXXX, XXX, XXX−XXX

of the probability density) in Figure 4c shows, the separation where negative torque is expected to be most prominent (that is around 400 nm center-to-center) is an unstable position, the transition region, between the more stable near-field and optical binding regions. We observe 125 occurrences (counts) at ∼400 nm separation versus 4×10^4 total measurements of particle separations in Figure 4c.

A trajectory where an EBD transitions from the near-field toward optical binding separations is shown in Figure 4d. The arrow indicates the transition point at 400 nm separation where the EBD briefly rotates in the direction opposite to the right-handed circular polarization. Until the transition point the particles are in the near-field regime and experience a strong positive torque manifested as a change in the EBD orientation corresponding to the handedness of the incident right CP light. On the other hand, beyond the transition region (around 400 nm separation) we see that the change in interparticle angle is small and averages to zero. At the transition point, the EBD orientation changes with opposite handed rotation, a signature of negative torque. Figure 4e shows the instantaneous value of ω as a function of interparticle separation for the trajectory in Figure 4d, which also demonstrates the transition from the near-field regime to the optical binding regime with a signature of negative torque during the transition. The experimental frames upon which Figures 4d,e are based are given in the Supporting Information and in Movie S6.

Figure 4f shows the experimentally measured average angular velocity plotted as a function of interparticle separation for a right-hand CP trapping beam. The mean velocity is large and positive for small nanoparticle separations, while it averages to zero at optical binding separations. We note that the mean ω is negative around 400 nm, at the transition between these regimes, as is expected from the ED−LD simulations of negative torque. The shaded regions define the standard deviation, with magnitude mostly due to Brownian fluctuations affecting the particle motion.

The mean ω value at the interparticle separation of ∼400 nm is −85 rad/s. We can establish the confidence in this result by statistically estimating the likelihood of observing this magnitude of negative torque for 125 events from simulated Brownian motion distributions matching our experimental conditions. This analysis, which is presented in detail in the Supporting Information, demonstrates that the experimental negative torque value is not due to Brownian fluctuations with a confidence level of 99.6%, approximately 3σ. We repeated the experiment on 200 nm diameter Ag nanospheres. Despite significant differences in particle scattering and trapping behavior compared to their 150 nm diameter counterparts we observed negative torque at 410 nm with a 2σ confidence level. The details of the experiment and its results and analysis are given in the Supporting Information.

Discussion and Conclusions. We have demonstrated through experiments and simulations the formation and concomitant rotation of electrodynamically bound dimers (EBD) about their center of mass using Ag nanoparticles trapped in focused circularly polarized Gaussian beams. The angular velocity of the EBDs increases linearly with the incident optical power. We present an analytical model for the effective polarizability of the EBD that predicts the existence of negative torque, that is, rotation of the EBD opposite to the direction of CP that stems from retardation of the scattered field and electrodynamic interactions between the particles. For the size of the particles (150 nm) we considered, the full ED−LD numerical simulations of the dynamics of the optical dimer are necessary for a quantitative comparison with experiments due to the excitation of higher-order modes in these particles and the small relative separations between them. We directly demonstrate the opposite handed rotation due to negative torque on the EBD in simulations. Using 4×10^4 measurements of EBDs trapped in a CP beam we were able to experimentally observe and statistically verify the signature of negative torque at the separations predicted by the theory and simulations.

Although the EBD can rotate with a handedness opposite to the incident field, the angular momentum in this system is conserved. It is known that a circularly polarized incident field can transfer angular momentum to a single spherical particle only via absorption.[35] In the case of a nonabsorbing spherical scattering particle, the angular momentum carried by the incident field is not transferred to the particle but rather distributed into the scattered fields. Moreover, in the far-field the angular momentum carried by the scattered fields depends on the direction,[36] for example, in the forward (backward) direction the helicity is positive (negative). In other words, an absorbing test particle placed in the forward direction of a scattering particle will spin with the same handedness as the incident polarization, while in the backward direction it will spin with negative (or opposite) handedness. At an arbitrary angle the scattered fields will contain linear combinations of positive (i.e., same helicity as the incident field), negative (i.e., opposite helicity of the incident field), and linear (i.e., no angular momentum) polarization components. In a realistic particle that absorbs as well as scatters, a fraction of the incident angular momentum would be converted toward spinning of the particle, while the remaining fraction would be distributed in the scattered fields with angle-dependent helicity. With the addition of a second particle, the picture becomes more complicated due to the interaction terms that are dependent on the separation between the particles. However, the total angular momentum carried by the incident field is still conserved and distributed into an absorption part and an angle-dependent scattered part. Therefore, a negative (or opposite handed) torque can result from scattered fields while preserving the total angular momentum.

It is of interest to compare the dependence of the optical torque we observe for EBDs to previous reports detailing the rotation and orientation of single nanowires[37] and nanorods.[15] For example, Yan et al.[37] used FDTD simulation results to calculate the forces on Ag nanorods and nanowires illuminated by a linearly polarized planewave at 45° to the particle axis and showed that the direction of torque switches when the incident wavelength changes from being longer to shorter than the particle's plasmon resonance; that is, as the particle changes from a nanorod to a nanowire. Likewise, the report by Tong et al.[15] described rotation of Ag nanorods and Au dimers by LP and CP beams, where the dimensions and material composition of the trapped particles determined its rotational direction and the trap stiffness. In both cases, the changes in torque direction are explained as an effect of the location of the plasmon resonance relative to the trapping wavelength.

The intriguing opposite handed rotation stemming from negative torque creates new opportunities to control the dynamics of multiparticle optical matter structures in CP light where near-field, optical binding, and intermediate separations could occur simultaneously and by working with materials and

DOI: 10.1021/acs.nanolett.7b02196
Nano Lett. XXXX, XXX, XXX−XXX

at wavelengths where the plasmon resonance effect and retardation are both employed.

■ ASSOCIATED CONTENT

Supporting Information

The Supporting Information is available free of charge on the ACS Publications website at DOI: 10.1021/acs.nanolett.7b02196.

Additional information about experimental setup; characteristics of 150 nm diameter Ag nanoparticles; simulation method; image analysis; total optical torque calculation; interaction matrix elements; converting fields to the coordinate frame of the EBD; relation between angular velocity and torque in an overdamped system; example of negative torque event; statistical analysis for negative torque; observation of negative torque in 200 nm Ag diameter nanoparticle EBDs (PDF)

Experimental video of two 150 nm diameter Ag nanoparticles trapped in the near-field region in a linearly polarized focused Gaussian beam (AVI)

Simulated trajectories of two 150 nm Ag nanoparticles illuminated by a circularly polarized focused Gaussian beam (both right-handed and left-handed circular polarization) (AVI)

Experimental video of two 150 nm diameter Ag nanoparticles trapped in a left-handed circularly polarized loosely focused Gaussian beam (AVI)

Experimental video of two 150 nm diameter Ag nanoparticles trapped in the near-field region and rotating clockwise in a right-handed circularly polarized focused Gaussian beam (AVI)

Experimental video of two 150 nm diameter Ag nanoparticles trapped in the near-field region and rotating counterclockwise in a left-handed circularly polarized focused Gaussian beam (AVI)

Example of a negative torque event taken from an experimental video of two 150 nm diameter Ag nanoparticles trapped in a left -handed circularly polarized loosely focused Gaussian beam (AVI)

■ AUTHOR INFORMATION

Corresponding Author

*E-mail: nfschere@uchicago.edu.

ORCID

Yuval Yifat: 0000-0003-0952-556X

Author Contributions

N.S and Y.Y. contributed equally to this work. N.S developed the simulation code and performed the simulations and theoretical analysis. Y.Y. designed and performed the experiment and conducted the data analysis. All authors participated in the writing of the manuscript.

Notes

The authors declare no competing financial interest.

■ ACKNOWLEDGMENTS

We thank Denise Hernandez and Edgar Duenas for the help in particle tracking of the experimental videos. We also thank Tian-Song Deng and Delphine Coursault for their help in the characterization experiments of the Ag nanoparticles. The authors acknowledge support from the Vannevar Bush Faculty Fellowship program sponsored by the Basic Research Office of the Assistant Secretary of Defense for Research and Engineering and funded by the Office of Naval Research through grant N00014-16-1-2502. This work was performed, in part, at the Center for Nanoscale Materials, a U.S. Department of Energy Office of Science User Facility, and supported by the U.S. Department of Energy, Office of Science, under Contract No. DE-AC02-06CH11357. We also thank the W.M. Keck Foundation for partial support of this research.

■ REFERENCES

(1) Ashkin, A.; Dziedzic, J. M.; Bjorkholm, J. E.; Chu, S. *Opt. Lett.* **1986**, *11*, 288−290.
(2) Grier, D. G. *Nature* **2003**, *424*, 810.
(3) Svoboda, K.; Block, S. M. *Annu. Rev. Biophys. Biomol. Struct.* **1994**, *23*, 247.
(4) Zhang, H.; Liu, K.-K. *J. R. Soc., Interface* **2008**, *5*, 671−690.
(5) Marago, O. M.; Jones, P. H.; Gucciardi, P. G.; Volpe, G.; Ferrari, A. C. *Nat. Nanotechnol.* **2013**, *8*, 807−819.
(6) Mcleod, E.; Arnold, C. B. *Nat. Nanotechnol.* **2008**, *3*, 413−417.
(7) Crocker, J. C.; Grier, D. G. *Phys. Rev. Lett.* **1994**, *73*, 352−355.
(8) Grier, D. G. *Curr. Opin. Colloid Interface Sci.* **1997**, *2*, 264−270.
(9) Li, T.; Kheifets, S.; Medellin, D.; Raizen, M. G. *Science* **2010**, *328*, 1673−1675.
(10) Figliozzi, P.; Sule, N.; Yan, Z.; Bao, Y.; Burov, S.; Gray, S. K.; Rice, S. A.; Vaikuntanathan, S.; Scherer, N. F. *Phys. Rev. E: Stat. Phys., Plasmas, Fluids, Relat. Interdiscip. Top.* **2017**, *95*, 022604.
(11) Bowman, R. W.; Padgett, M. J. *Rep. Prog. Phys.* **2013**, *76*, 026401.
(12) Friese, M. E. J.; Nieminen, T. A.; Heckenberg, N. R.; Rubinsztein-Dunlop, H. *Nature* **1998**, *394*, 348−350.
(13) Bishop, A. I.; Nieminen, T. A.; Heckenberg, N. R.; Rubinsztein-Dunlop, H. *Phys. Rev. Lett.* **2004**, *92*, 198104.
(14) Pelton, M.; Liu, M.; Kim, H. Y.; Smith, G.; Guyot-Sionnest, P.; Scherer, N. F. *Opt. Lett.* **2006**, *31*, 2075−2077.
(15) Tong, L.; Miljković, V. D.; Käll, M. *Nano Lett.* **2010**, *10*, 268−273.
(16) Lehmuskero, A.; Ogier, R.; Gschneidtner, T.; Johansson, P.; Käll, M. *Nano Lett.* **2013**, *13*, 3129−3134.
(17) Haefner, D.; Sukhov, S.; Dogariu, A. *Phys. Rev. Lett.* **2009**, *103*, 173602.
(18) Kudo, T.; Wang, S. F.; Yuyama, K. I.; Masuhara, H. *Nano Lett.* **2016**, *16*, 3058−3062.
(19) Sbalzarini, I. F.; Koumoutsakos, P. *J. Struct. Biol.* **2005**, *151*, 182−195.
(20) Burov, S.; Figliozzi, P.; Lin, B.; Rice, S. A.; Scherer, N. F.; Dinner, A. R. *Proc. Natl. Acad. Sci. U. S. A.* **2017**, *114*, 221.
(21) Yifat, Y.; Sule, N.; Lin, Y.; Scherer, N. F. 2017, arXiv:1705.07789 (accessed October 3, 2017).
(22) Sule, N.; Rice, S. A.; Gray, S. K.; Scherer, N. F. *Opt. Express* **2015**, *23*, 29978−29992.
(23) Sun, W.; Pan, S.; Jiang, Y. *J. Mod. Opt.* **2006**, *53*, 2691−2700.
(24) Kong, S. C.; Simpson, J. J.; Backman, V. *IEEE Microwave and Wireless Components Letters* **2008**, *18*, 4−6.
(25) Novotny, L.; Hecht, B. *Principles of Nano-Optics*; Cambridge University Press: Cambridge, 2006; pp 45−88.
(26) O'Neil, A. T.; MacVicar, I.; Allen, L.; Padgett, M. J. *Phys. Rev. Lett.* **2002**, *88*, 053601.
(27) Emile, O.; Emile, J. *Opt. Lett.* **2016**, *41*, 211−214.
(28) Yan, Z.; Gray, S. K.; Scherer, N. F. *Nat. Commun.* **2014**, *5*, 3751.
(29) Dholakia, K.; Zemánek, P. *Rev. Mod. Phys.* **2010**, *82*, 1767−1791.
(30) Khlebtsov, B.; Melnikov, A.; Zharov, V.; Khlebtsov, N. *Nanotechnology* **2006**, *17*, 1437−1445.
(31) Pinchuk, A.; Schatz, G. *Nanotechnology* **2005**, *16*, 2209.
(32) Chaumet, P. C.; Billaudeau, C. *J. Appl. Phys.* **2007**, *101*, 023106.
(33) Simpson, S. H.; Hanna, S. *J. Opt. Soc. Am. A* **2009**, *26*, 625−638.
(34) Chen, J.; Ng, J.; Ding, K.; Fung, K. H.; Lin, Z.; Chan, C. T. *Sci. Rep.* **2015**, *4*, 6386.

DOI: 10.1021/acs.nanolett.7b02196
Nano Lett. XXXX, XXX, XXX−XXX

(35) Marston, P. L.; Crichton, J. H. *Phys. Rev. A: At., Mol., Opt. Phys.* **1984**, *30*, 2508.
(36) Dogariu, A.; Schwartz, C. *Opt. Express* **2006**, *14*, 8425−8433.
(37) Yan, Z.; Sweet, J.; Jureller, J. E.; Guffey, M. J.; Pelton, M.; Scherer, N. F. *ACS Nano* **2012**, *6*, 8144−8155.

DOI: 10.1021/acs.nanolett.7b02196
Nano Lett. XXXX, XXX, XXX−XXX